Ravishankar et al. *NPG Asia Materials* (2023) 15:1
https://doi.org/10.1038/s41427-022-00453-w

NPG Asia Materials

ARTICLE Open Access

Protein nanoparticle cellular fate and responses in murine macrophages

Samyukta Ravishankar[1], Anu Maashaa Nedumaran[2], Archana Gautam[2], Kee Woei Ng[2,3], Bertrand Czarny[2,4] and Sierin Lim[1,5]

Abstract

Nanoparticles (NPs), both organic and inorganic, have been identified as tools for diagnostic and therapeutic (theranostic) applications. Macrophages constitute the first line of defense in the human body following the introduction of foreign antigens, including nanoparticles. However, there is a limited understanding of the cellular fate and trafficking of organic NPs in macrophages as well as the molecular responses that are triggered. This knowledge is crucial for the effective translation of these engineered molecules for theranostic applications. In this work, we performed an in-depth study on the intracellular fate and relevant immune responses of a model organic NP, *Archaeoglobus fulgidus* ferritin, in murine macrophage (RAW264.7) cells. Ferritin, a naturally occurring iron storage protein, has been reported to target tumors and atherosclerotic lesion sites. Herein, we demonstrate a concentration-dependent internalization mechanism and quantify the subcellular localization of ferritin NPs in various organelles. After NP exposure, export of the iron present in the ferritin core occurred over an extended period of time along with upregulation of iron-related gene mRNA expression. A study on the modulation of the intracellular localization of the NPs was conducted by incorporating peptides to mediate endosomal escape and examining their molecular effects using transcriptional analysis. To further investigate the physiological effects, we monitored the upregulation of immune-related markers (i.e., CCR2, IL1β, TNFα, VCAM-1) along with ROS generation in cells treated with ferritin under various conditions. The in-depth analyses of cellular uptake and responses to versatile protein NPs, such as ferritin, provide basic principles to design and engineer other protein NPs with similar properties for future biomedical applications.

Introduction

Nanoparticles (NPs) have been recognized for their uses as therapeutic agents, imaging agents, and scaffolds for biomedical applications[1]. Macrophages are part of the innate immune system that constitute the first line of defense in response to the introduction of antigens in the human body. Activation of these innate immune cells results in the uptake of NPs and subsequent clearance or inflammatory response[2–4]. Macrophages are actively being studied as targets for the development of therapeutic NPs due to their activation at tumor and atherosclerotic sites[5,6]. Thus, understanding pathways by which NPs are taken up by macrophages, their intracellular trafficking and the resulting cellular responses remain a key research area. Elucidating these mechanisms will allow tuning of the physiochemical properties of NPs to achieve the desired bioavailability, ensure safety and fulfill the intended therapeutic or diagnostic function with improved efficacy.

The internalization pathways of synthetic NPs, such as superparamagnetic iron oxide nanoparticles (SPIONs) and gold NPs, have been extensively studied in macrophages and similar immune cells. SPIONs are internalized by time-dependent vesicle-bound pathways, resulting in

Correspondence: Sierin Lim (SLim@ntu.edu.sg)
[1]School of Chemistry, Chemical Engineering and Biotechnology, Nanyang Technological University, Jurong West, Singapore
[2]School of Materials Science and Engineering, Nanyang Technological University, Jurong West, Singapore
Full list of author information is available at the end of the article

the formation of multivesicular bodies in the cytoplasm. It has been accepted that some internalized SPIONs undergo lysosomal degradation, while others are released into the cytoplasmic compartments for further metabolism[7]. Other studies have demonstrated that the size and shape of NPs, such as gold NPs, affect their rate of uptake by HeLa cells[8–10]. Nature-derived NPs, such as protein NPs, lipoproteins, and viral capsids, are actively being developed as drug carriers to treat cancer and atherosclerosis, wherein the leaky vasculature allows for the permeation and accumulation of these NPs at the sites of interest[11–13]. Organic NPs generally have higher cellular uptake and degrade in vivo in the presence of proteolytic enzymes, thus overcoming potential toxicity issues[14,15]. Their uniform size distribution and facile production methods make organic NPs attractive molecules for applications in nanomedicine[16]. Similar to inorganic NPs, organic NPs are taken up by the reticuloendothelial system, wherein macrophages play a key role in engulfing and breaking down the injected NPs. Furthermore, in diseases such as atherosclerosis, NP uptake by vascular macrophages has been shown to facilitate their localization at the lesion site[17]. However, quantitative studies on the cellular fate of organic NPs have been largely limited due to challenges with detection of the particles in vitro.

Our work addresses this gap by using a quantitative method to investigate the uptake and trafficking mechanisms of organic NPs, specifically ferritin. In nature, ferritin stores insoluble ferric (Fe^{3+}) iron in a soluble and bioavailable form in the core of its cage-like structure. The encapsulation of iron into the core of the protein shell prevents its exposure to reactive oxygen species (ROS), thereby minimizing iron-induced oxidative damage. In recent decades, due to their inherent and tunable iron storage properties, ferritin has emerged as a major candidate in nanomedicine research, where it is often referred to as ferritin protein nanocages or ferritin NPs. These nanomaterials have been actively studied for applications as nanocarriers for iron-based contrast agents. Ferritin redox sites and ferroxidase centers serve as platforms for iron core formation with superparamagnetic properties and T2 relaxivity comparable to those of SPIONs while loading with manganese in its core enhances T1 relaxivity[18,19]. Several studies have demonstrated the passive localization of ferritin to lesion sites, such as in the case of tumors and atherosclerotic plaques[17,20–24]. Ferritin entry into cells has been shown to be mediated by the transferrin receptor (TfR1) and a scavenger receptor (Scara5), resulting in its localization to the endosomal and lysosomal compartments[25,26]. However, questions remain regarding the fate of ferritin in cells following internalization[16]. It has been commonly accepted that the protein shell undergoes lysosomal degradation in the presence of proteases at low pH. The iron in the protein core, however, is expected to undergo minimal degradation under these conditions. To our knowledge, no studies have elucidated the cellular fate of these iron nanoparticles encapsulated within a ferritin cage after internalization.

In this work, ferritin derived from *Archaeoglobus fulgidus* with two amino acid substitutions (K150A/R151A; AfFtnAA) served as the model organic NP. *A. fulgidus* ferritin comprises 24 polypeptides that self-assemble to form a ~12 nm cage structure in the presence of iron or high ionic concentrations[27,28]. In a standard protocol in this work, the twenty-four subunits assemble using 2400 Fe atoms ((Fe2400)AA) to form the cage structure. AfFtnAA is a closed-pore mutant with iron-mediated tunable self-assembly and facile surface modification properties[28,29]. The thermophilic source imparts the protein with high thermostability, which remains despite the amino acid substitutions[30,31]. *Af* ferritin presents distinct advantages over human ferritin, which gives low yield upon peptide modification[32]. The iron-mediated self-assembly properties of human ferritin are also distinct from those of *Af* ferritin. Mammalian ferritin requires pH-mediated disassembly/reassembly to encapsulate non-native cargos and form cage structures, which often results in lower yield upon assembly compared with *Af* ferritin[33]. The Fe atoms located in the ferritin core are used for quantification (measured using inductively coupled plasma–mass spectrometry) to monitor the cellular trafficking of ferritin NPs and their subsequent degradation. Herein, we show a concentration-dependent ferritin NP internalization pathway in RAW264.7 murine macrophages. The observed dominant lysosomal and cytoplasmic localization of iron is followed by its export from cells in a time-dependent manner. The internalization of ferritin NPs affects iron homeostasis in cells at the transcriptional level, with observed changes in iron-related proteins and endogenous ferritin levels. To further understand the impact of subcellular localization on cellular iron homeostasis mechanisms, we modified ferritin NPs to direct their localization. We assessed the expression of immune-related genes and intracellular oxidative stress in response to ferritin NP treatment and explored methods to counter the responses. Lastly, an in vivo study of ferritin NP accumulation in macrophage-laden atherosclerotic plaques is reported.

Results

In vitro demonstration of ferritin NP internalization by macrophages

To visualize the internalization of ferritin NPs into macrophages, confocal imaging was carried out using FITC-conjugated AfFtnAA (green) and LysoTracker (red). The regions with overlapping green and red fluorescence are indicative of intracellular ferritin NP colocalization (Fig. 1).

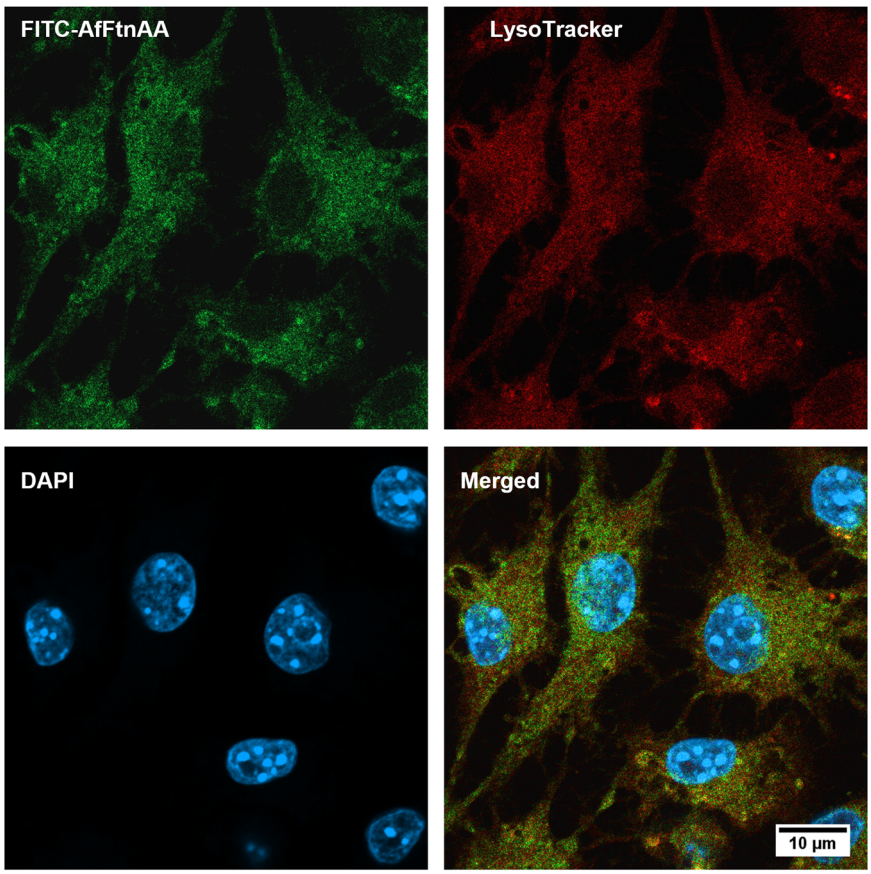

Fig. 1 Confocal imaging of 200 nM FITC (green)-conjugated AfFtnAA uptake by RAW264.7 cells after 24 h of incubation. Cells were stained with DAPI (blue) and LysoTracker (red) to visualize the nuclei and lysosomal compartments, respectively.

The images reveal that ferritin NPs localize in the endosomal/lysosomal compartments. However, nonspecific staining around the cellular compartments causes difficulties in distinguishing the individual organelles. Treatment of the cells with ferritin NPs for 1 h at 4 °C results in localization of the cages on the membrane along with some internalized particles (Fig. S1). The binding of ferritin NPs to the cell membrane under stunted uptake conditions (lower temperature, 4 °C) indicates internalization pathways that are mediated by membrane interactions/binding. To further discern the cellular compartments into which the ferritin NPs were internalized, ICP–MS was used to study the mechanism by monitoring the amount of Fe present in the organelles that were individually isolated from the whole cell lysate.

Ferritin NP internalization involves more than a single dominant pathway

To determine the dominant endocytosis pathway, cells were incubated with 2 nM and 200 nM ferritin NPs in the presence of the inhibitors chlorpromazine hydrochloride, genistein and amiloride hydrochloride hydrate for clathrin-mediated endocytosis, caveolae-mediated endocytosis and macropinocytosis, respectively, for 2 h under typical cell culture conditions. The percent cellular uptake was normalized to ferritin NP uptake in the absence of inhibitor (Fig. 2A). At the lower concentration of ferritin NPs, the greatest inhibition of uptake (29%) was observed for the macropinocytosis pathway, and the lowest inhibition (8%) was for the clathrin-mediated endocytosis pathway. In contrast, at the higher ferritin NP concentration, uptake inhibition was observed to a similar extent of ~15–22% with all three inhibitors. Thus, at both concentrations, ferritin NP internalization appeared to be mediated by more than one pathway. However, a NP concentration of approximately 200 nM was required for clathrin-coated pits to play a role in mediating uptake along with the caveolae pits and macropinosomes.

The overall ferritin NP uptake in cells was further monitored by treatment over extended periods of time. A steady rise in Fe accumulation per cell was observed over 24 h while the Fe content in untreated cells remained stagnant (Fig. 2B). The significant drop at 48 h,

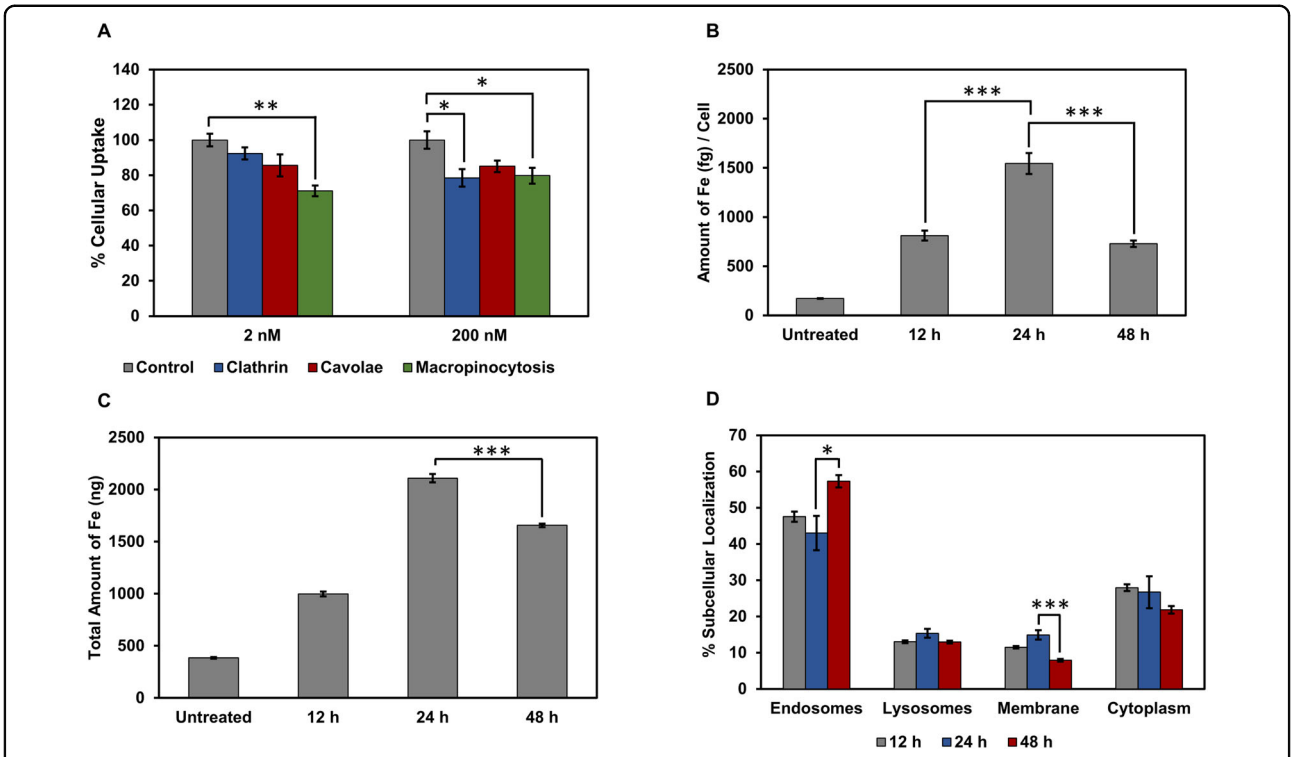

Fig. 2 Endocytosis pathway and localization. A Endocytosis pathway determined with cells incubated with 200 nM AfFtnAA for 2 h in the presence of inhibitors to test for clathrin-mediated endocytosis, caveolae-mediated endocytosis and macropinocytosis. **B** Amount of Fe accumulated per cell. **C** Total amount of Fe per well in cells incubated with 200 nM AfFtnAA for 12, 24 and 48 h. Untreated cells were not incubated with AfFtnAA ($n = 3$). **D** Percent Fe distribution measured in the endosomes, lysosomes, membranes, and cytoplasm in cells incubated with AfFtnAA for 12, 24 and 48 h ($n = 2$). The percent localization was calculated based on the total amount of Fe detected per cell (*$p < 0.05$, **$p < 0.01$, ***$p < 0.005$).

suggested that the rate of mitosis exceeded the rate of AfFtnAA uptake. Additionally, a decrease in total Fe levels in cells treated with ferritin NPs for 48 h was observed (Fig. 2C). This observation indicates possible iron export with increased exposure time to maintain iron homeostasis.

To understand iron trafficking in the cellular compartments after ferritin NP internalization, we performed density ultracentrifugation to isolate endosomes, lysosomes, the cell membrane, and the cytoplasm (Fig. 2D). The percent distribution was calculated with respect to the total amount of Fe measured from these organelles combined. After 24 h of treatment at 37 °C, 43% of the Fe was present in the endosomal vesicles, followed by 27% in the cytoplasmic region. Within 24 h, minimal changes in localization were observed across the organelles. After 48 h, the endosomal iron content increased to 57%, and the cell membrane accumulation decreased. Membrane interaction/binding has been previously identified as the initial step prior to internalization[1,34]. The decreased Fe content in the membrane preparation thus indicated less membrane interactions following gradual Fe saturation with the extended time. Furthermore, an increase in endosomal Fe levels suggested the formation of endosome-sized vesicles to mediate iron export.

Ferritin NPs are visualized in the cytoplasm and undergo degradation in the lysosomal environment

The cellular compartment localization of the ferritin NPs was further visualized using transmission electron microscopy (TEM). Cells treated with ferritin NPs for 24 h were compared to untreated cells (Fig. 3). In the cytoplasm, a few electron-dense black particles corresponding to the iron cores of ferritin NPs were identified, and these particles were absent in untreated cells. The observed high-contrast particles were expected to be aggregated ferritin particles (not having undergone endosomal/lysosomal degradation), thus differing in size from the average hydrodynamic diameter of ferritin (12–15 nm). However, no such particles were observed in the endosomal, lysosomal or other cytoplasmic compartments even though the presence of iron was detected in these organelles from previous ICP–MS measurements. This is likely due to the degradation of the protein and iron core structures in the lysosomal compartment, resulting in a pool of free Fe ions that cannot be observed by electron microscopy.

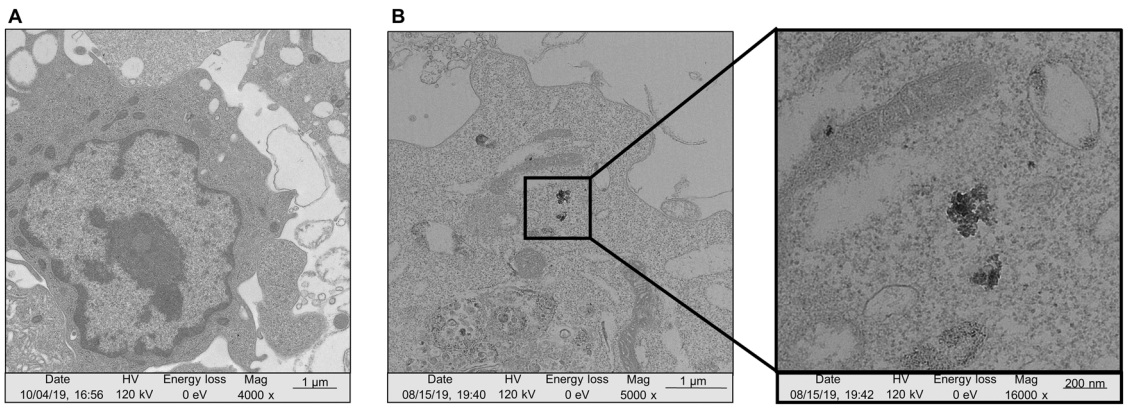

Fig. 3 Transmission electron micrographs of RAW264.7 cells. The samples were (**A**) untreated and (**B**) treated with 200 nM AfFtnAA for 24 h. Scale bars are 1 µm (magnified image scale bar is 200 nm).

To further study the lysosomal degradation mechanism of ferritin NPs, the lysosomal environment was simulated in vitro. The fusion of endosomes with lysosomal compartments typically involves a decrease in pH, the presence of lysosomal enzymes and reducing conditions[35,36]. Since endolysosomal fusion is often a dynamic process, the above three variables were studied independently to understand the ferritin NP degradation pathway. The integrity of the cage structure was visualized using TEM under different buffer conditions (Fig. 4A–D). Stained and unstained samples were used to visualize the intactness of the protein shell and iron core, respectively. As can be seen from the unstained electron micrographs, dissolution of the iron core occurs in a reducing environment (EDTA and DTT). However, complete dissociation of the protein shell was not noted at the reducing agent concentrations tested in this study. The dissolution rate of the iron core was further studied by measuring the iron release kinetics. As the Fe^{3+} in the core was reduced to Fe^{2+} and dissolved, the released free ions formed a complex with ferrozine. The absorbance signal resulting from complex formation was monitored to determine the iron release rate (Fig. 4E). Iron core dissolution occurred within 10 min of exposure to the reducing environment, with a maximum of 600 µM Fe (~60% of the total Fe content in the cage) released under low pH and reducing conditions at 37 °C. No iron was observed to be released from ferritin under neutral or low pH conditions in the absence of reducing agents, indicating the intactness of the core structure within. Cathepsin-B was the lysosomal enzyme chosen to mimic the lysosomal environment due to its dual endo- and exopeptidase activities under neutral and low pH conditions, respectively[37]. The iron release kinetics measurements showed that the degradation of the core plateaued after 12 h (Fig. 4F). Thus, degradation in the presence of cathepsin-B occurred at a slower rate than that under reducing conditions. More Fe ions release were detected after exposure to the enzyme at pH 7.4 than at pH 5.0. This was further validated using TEM, where higher numbers of intact cages and the corresponding iron cores were observed under low pH conditions. Extended degradation studies in the presence of varying concentrations of lysosomal enzyme can be conducted to elucidate the comparative effects of the endopeptidase and exopeptidase activity of cathepsin-B on ferritin. Since under all conditions the iron cores dissolved after protein shell degradation, it was concluded that the high-contrast particles observed in the endosomal compartments corresponded to intact ferritin NPs.

Iron homeostasis in cells treated with ferritin NPs

The effect of exogenous ferritin NP treatment on endogenous proteins involved in maintaining iron homeostasis was investigated using real-time quantitative polymerase chain reaction (RT-qPCR) (Fig. 5A). The primers used for all reactions are summarized in Table S1. The mRNA expression levels of endogenous mammalian L- and H-ferritin were monitored. The fold changes in the mRNA expression levels of the target proteins were normalized to untreated cells. Seven- and 9-fold increases in the mRNA levels of L-ferritin and H-ferritin were measured after 48 h of treatment. Upregulation of ferroportin, an iron exporter protein, was also observed, but not to the same extent.

To investigate the possibility of Fe export, Fe levels were monitored intracellularly and in media (Fig. 5B). Following cell treatment with ferritin NPs for 24 h at 37 °C, the culture media was replaced to remove excess NPs. Iron levels were then monitored for 24 h after medium change. An overall 30% decrease in intracellular Fe levels was observed to gradually occur over 24 h. Correspondingly, an increase in Fe levels in the culture medium was measured, indicating that iron was released from the cells into the extracellular environment, likely by exocytosis.

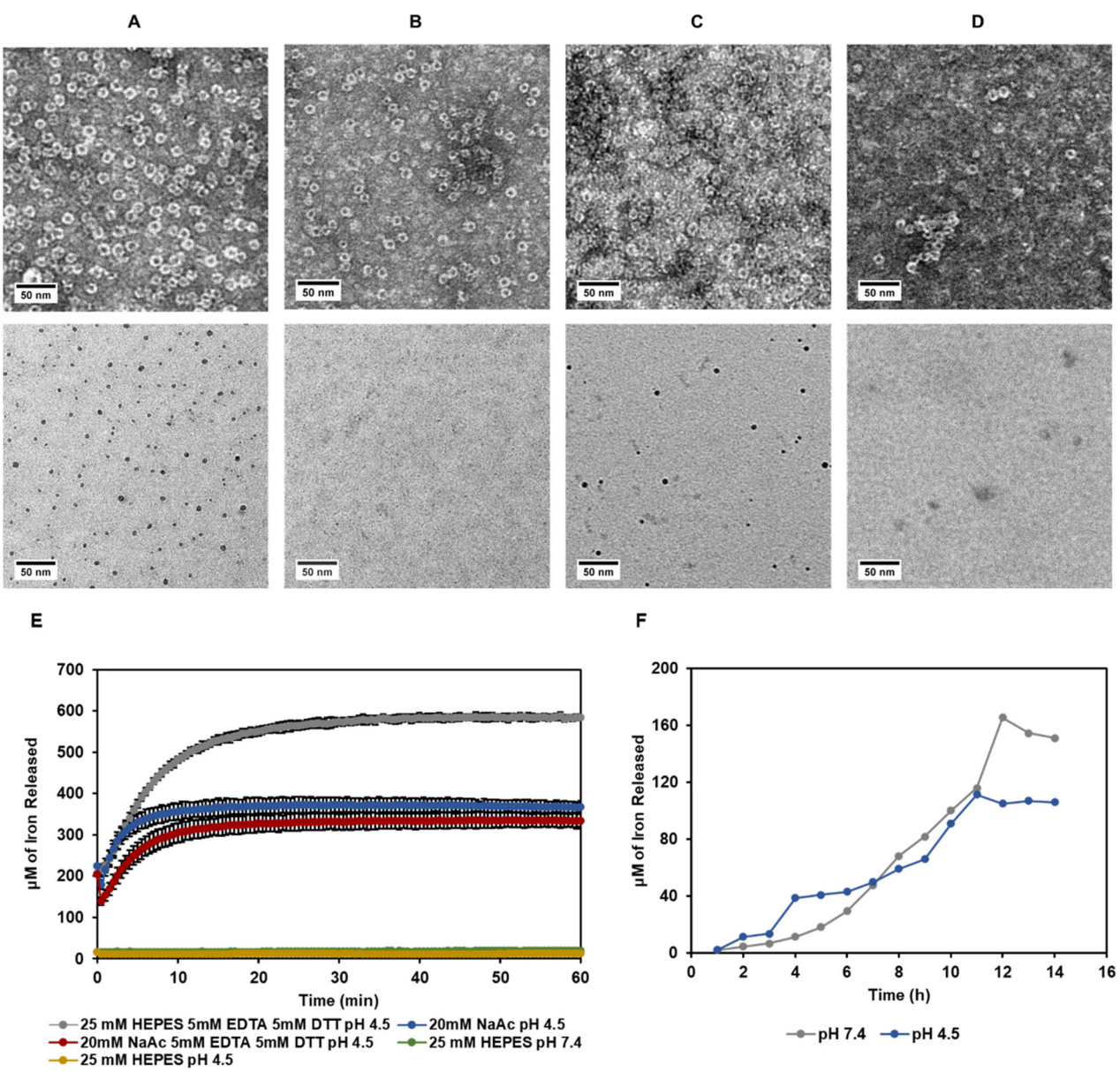

Fig. 4 Structural analyses and iron release of AfFtnAA in lysosomal degradation condition in vitro. A–D Transmission electron micrographs (top row—stained, bottom row—unstained) demonstrating lysosomal degradation. AfFtnAA in the presence of (**A**) 25 mM HEPES, pH 7.4; (**B**) 20 mM NaAc, 5 mM DTT, 5 mM EDTA, pH 4.5; (**C**) 25 mM HEPES, 1 unit of cathepsin-B, pH 4.5; and (**D**) 25 mM HEPES, 1 unit of cathepsin-B, pH 7.4. **E** Cumulative iron release after incubation with AfFtnAA under different reducing/nonreducing conditions for 1 h ($n = 3$, where n is the number of repeats conducted for each experimental condition). **F** Cumulative iron release after incubation with AfFtnAA in the presence of the lysosomal enzyme cathepsin-B at pH 7.4 and pH 4.5 for 14 h.

Ferritin NP treatment induces cellular responses and oxidative stress

To elucidate the immune response of RAW264.7 cells to ferritin NP treatment, the mRNA expression levels of the related genes were determined (Fig. 6A). These included proinflammatory cytokines (TNFα and IL1β), a chemokine (CCR2) and vascular cell adhesion molecule (VCAM-1), which is responsible for leukocyte signaling and adhesion. The aforementioned genes were selected to represent cellular stress and responses in macrophages upon incubation with ferritin NPs[38]. Ferritin NP treatment had no significant effects on TNFα, CCR2, and VCAM-1 expression; however, within the 24 h of exposure, significant upregulation (~6500-fold change) of IL1β was observed. To further study the upregulation of this cytokine, an experiment investigating the

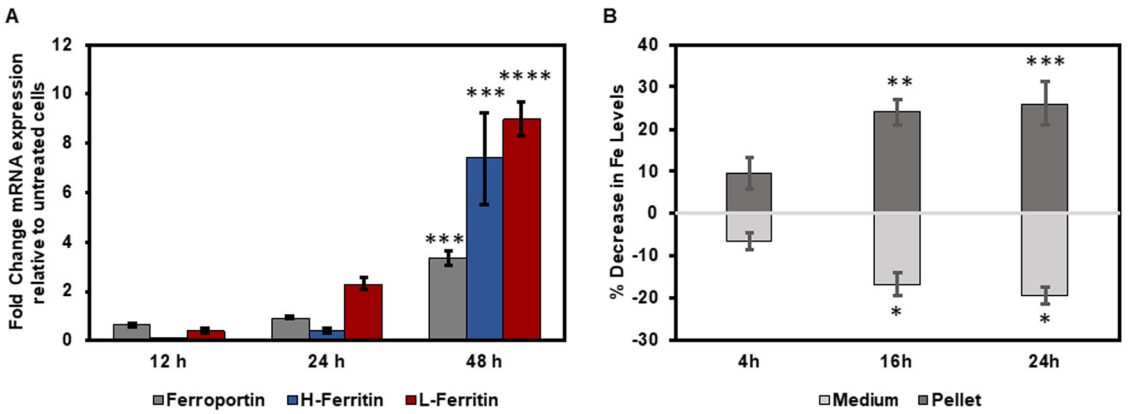

Fig. 5 Quantification of mRNA expression and iron levels of RAW264.7 in the presence of AfFtnAA. A mRNA expression levels of ferroportin, H-ferritin and L-ferritin in macrophages in the presence of 200 nM AfFtnAA for 12, 24 and 48 h. The mRNA expression levels were calculated relative to control samples without AfFtnAA treatment. **B** Decreases in the intracellular (pellet) Fe levels and medium measured at 4, 16 and 24 h. The change was calculated in reference to cells and medium at the 0 h timepoint ($n = 3$) (*$p < 0.05$, **$p < 0.01$, ***$p < 0.005$, ****$p < 0.001$). Significance values are represented with respect to the untreated control samples for (**A**) and with respect to the 0 h timepoint for (**B**).

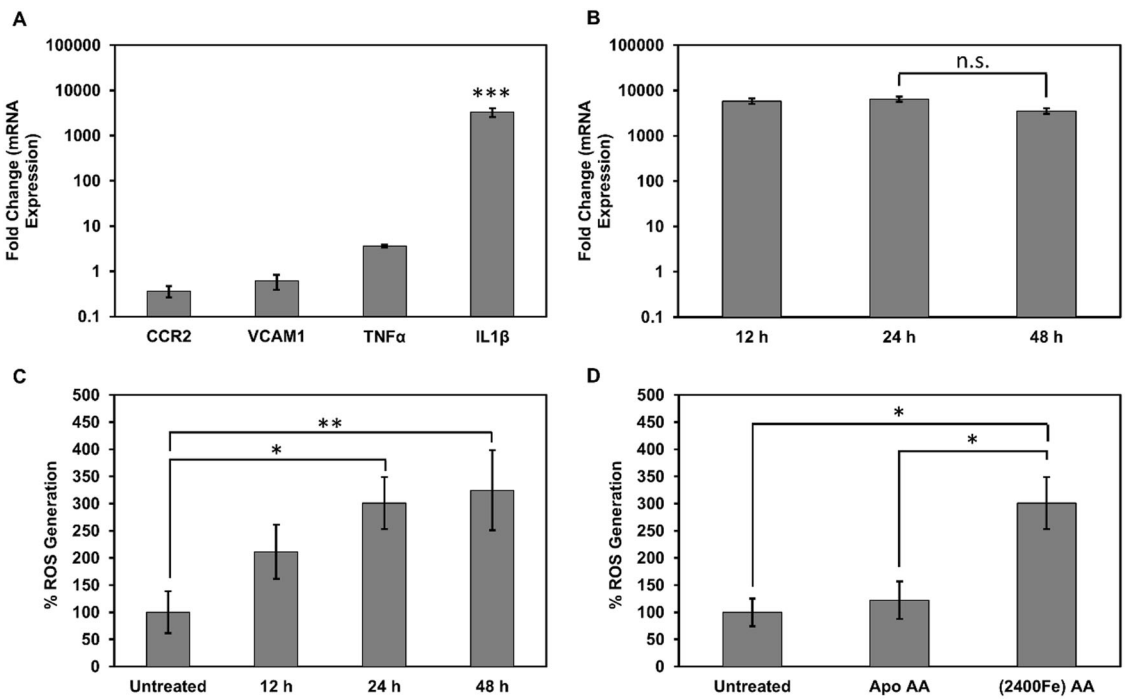

Fig. 6 Immunogenic responses of RAW264.7 to AfFtnAA treatment. A mRNA expression levels of cytokines and chemokines (CCR2, VCAM-1, TNFα and IL1β) in RAW264.7 cells treated with AfFtnAA for 48 h. **B** Time-dependent IL1β mRNA expression level changes in cells treated with 200 nM AfFtnAA (12, 24, 48 h). The expression levels of the target genes were normalized to those of untreated cells to determine the fold change. **C** Measurements of ROS generation in cells treated with AfFtnAA for different lengths of time (12, 24, 48 h). **D** Measurements of ROS generation in cells treated with ApoAA and iron-loaded AfFtnAA for 24 h. The ROS generated (measured as mean fluorescence intensity) is expressed as a percentage with respect to the mean fluorescence of the untreated cells ($n = 3$) (*$p < 0.05$, **$p < 0.01$, ***$p < 0.005$).

time-dependent exposure to ferritin NPs was carried out for 12, 24 and 48 h (Fig. 6B). The mRNA expression levels peaked by 12 h of treatment without significant changes afterwards.

To further understand the stress induced in cells treated with ferritin NPs, the generation of reactive oxygen species (ROS) was quantified using dihydroethidium (DHE) as the fluorescent probe. The measured mean fluorescence

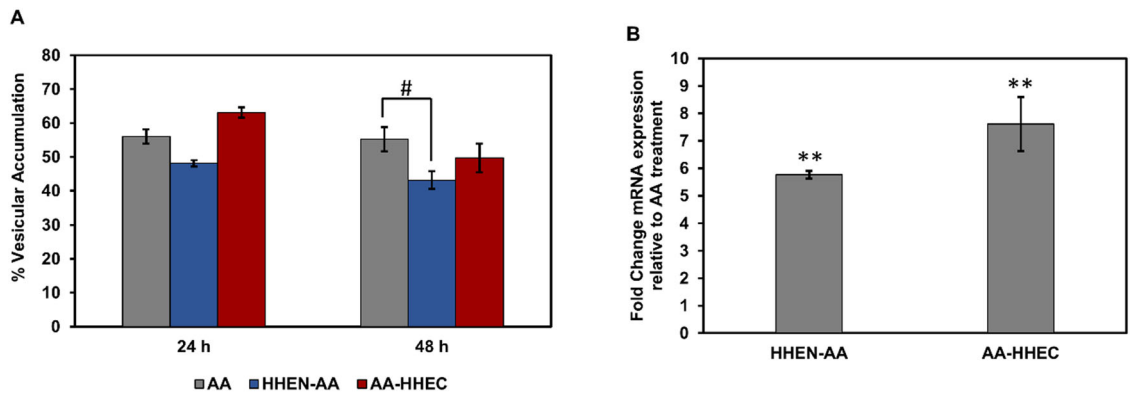

Fig. 7 Poly-histidine-tagged ferritin protein nanocages. A Percent Fe accumulation in the endosomal/lysosomal vesicular compartments in cells incubated with 75 nM AA, HHEN-AA and AA-HHEC for 24 and 48 h. The percentages were calculated relative to the total amount of Fe measured in the endosomal/lysosomal, cytoplasmic and membrane compartments. **B** mRNA expression levels of L-ferritin in macrophages in the presence of 75 nM HHEN-AA and AA-HHEC for 48 h. The mRNA expression levels were calculated relative to those in cells treated with AfFtnAA ($n = 3$) ($^{\#}p < 0.1$, $^{**}p < 0.01$).

intensity of the treated samples was normalized to that of the untreated samples to determine the % ROS generated. A time-dependent increase in ROS was observed, with the highest increase reaching 324% with prolonged (48 h) ferritin NP treatment (Fig. 6C). The generation of free radicals was hypothesized to be due to the Fe^{3+} ions loaded into the ferritin core undergoing the Fenton reaction following protein shell degradation in lysosomes. To confirm that the presence of iron caused the increase in ROS, a comparison was drawn between two types of ferritin NPs, ApoAA and (Fe2400)AA (Fig. 6D). ApoAA do not have an iron core but assembles in the presence of 500 mM sodium chloride as opposed to conventional Fe^{2+}-mediated assembly. Significantly lower ROS levels, close to those in the untreated samples, were observed after 24 h of ApoAA treatment compared to (Fe2400)AA-treated samples. A similar trend was observed with the mRNA expression levels of IL1β, which were lower after ApoAA exposure compared to iron-loaded ferritin NP treatment (Fig. S2A). This observation indicates that the Fe within the cages induces cellular stress and immune-related responses.

Poly-histidine modification mediates endosomal escape of ferritin NPs and subsequent transcriptional effects on endogenous ferritin levels

To facilitate ferritin NP escape from the endosomes for redirection to the cytosol, ferritin NPs (AfFtnAA; referred to as AA in this section) were genetically engineered to display poly-histidine peptides on their outer surface (HHEN-AA) and within their inner cavity (AA-HHEC). The poly-histidine peptide comprises nine repeats of HHE amino acid. The intermittent placement of glutamic acid residues lowers the hydrophobicity of the histidine-rich peptide, thereby enhancing the overall protein solubility[39]. The engineered ferritin NPs were expressed and purified following the same method that was used for the unmodified ferritin NPs with slight modification of the heat treatment step (75 °C instead of 85 °C) to ensure protein stability (Fig. S3A–C). Cage formation was mediated with 1200 Fe atoms as opposed to 2400 Fe atoms in previous experiments to maximize protein stability. TEM and ICP–MS analyses revealed that the poly-histidine modification placed near the inner cavity aided in higher Fe loading per cage, which was likely due to the electrostatic interactions between the glutamic acid residues and Fe^{2+} ions at the iron loading step. Similar observations have been previously reported for E2 protein nanocages[40]. The Fe core sizes were correspondingly larger for AA-HHEC than for HHEN-AA and unmodified AA (Fig. S4). Next, cells were incubated with 75 nM poly-histidine-modified AA or control unmodified AA for 24 h and 48 h. Fe accumulation was measured in the lysosomal/endosomal compartments and quantified with respect to the combined total Fe content measured from other cellular organelles, such as the vesicular compartments, membrane, and cytoplasm.

Ten percent and 5% decreases in endosomal/lysosomal Fe accumulation were observed in cells treated with HHEN-AA and AA-HHEC, respectively, compared to unmodified AA (Fig. 7A). The longer treatment time resulted in greater endosomal/lysosomal escape and redistribution to the cytoplasmic compartments. Six-fold greater endogenous L-ferritin mRNA expression levels were observed after 48 h of treatment with both poly-histidine modified protein conjugates compared to unmodified AA (Fig. 7B). The fold change values were estimated based on cells treated with equimolar amounts of unmodified AA for 48 h. The RT–qPCR results showed that a slight increase in cytoplasmic

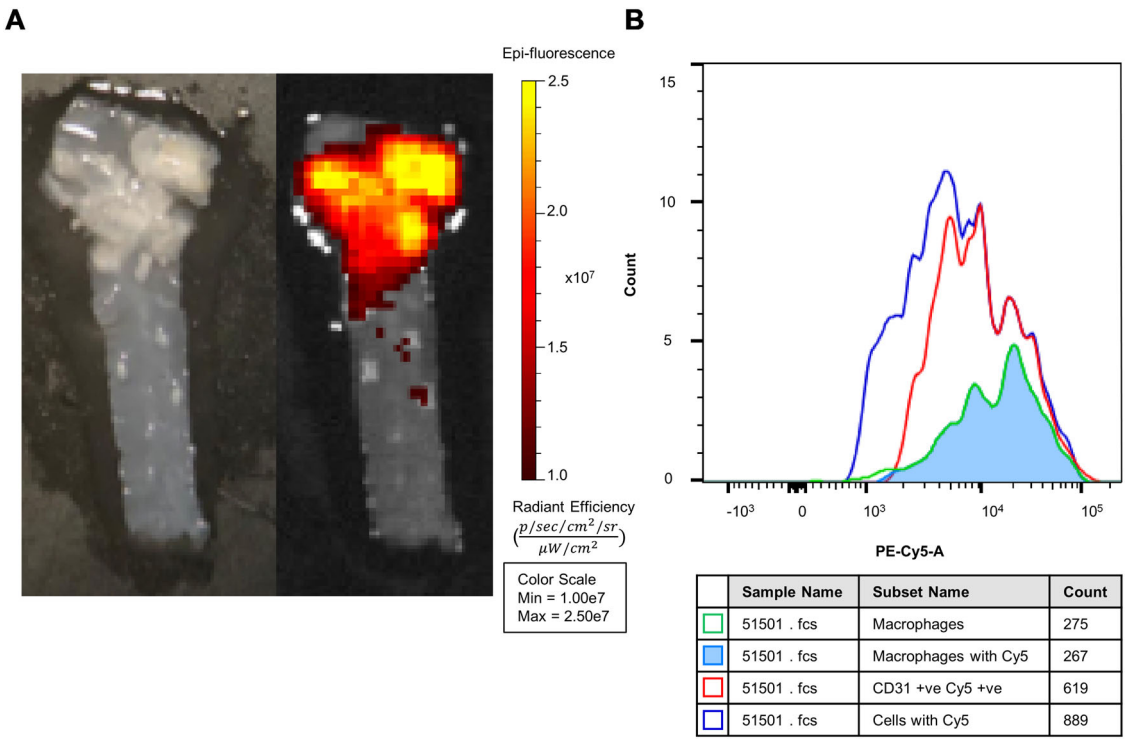

	Sample Name	Subset Name	Count
	51501 . fcs	Macrophages	275
	51501 . fcs	Macrophages with Cy5	267
	51501 . fcs	CD31 +ve Cy5 +ve	619
	51501 . fcs	Cells with Cy5	889

Fig. 8 Localization of AfFtnAA in atherosclerotic lesion sites. A Optical photograph and ex vivo fluorescence image obtained from IVIS of the aorta 1 h after mice were injected with Cy5-conjugated AfFtnAA. **B** Flow cytometry of the aorta samples indicating Cy5-positive cells (blue) and CD31-positive cells (red). The total number of macrophages present and the number of Cy5-positive macrophages are shown in green and as shaded blue areas, respectively.

Fe levels could alter the endogenous mRNA expression levels of ferritin.

In vivo ferritin NP localization in macrophage-rich atherosclerotic lesion sites

The localization of ferritin NPs in macrophages was further investigated in vivo using apolipoprotein E (ApoE) knockout ($ApoE^{-/-}$) mouse models with induced atherosclerotic lesions. The lesion sites were expected to comprise proinflammatory macrophages in the aortic region. Atherosclerotic plaques were induced in $ApoE^{-/-}$ mice by feeding them a high-fat diet. Ferritin NPs conjugated with cyanine 5 (Cy5) dye were used to visualize ferritin NP localization. Within 1 h of injection, fluorescence signals were observed in the lesion site in the aorta (Fig. 8A), and minimal fluorescence signals were measured in the blood and urine within the 1 h time period. Preliminary biodistribution studies elucidated that renal and hepatic clearance of ferritin occurred, as visibly high fluorescence intensities were measured in the liver, intestine, and kidneys (Fig. S5). Flow cytometry analysis of the digested aortas showed that 82% of the total event population identified as cells were positive for Cy5. Among the Cy5-positive cells, 70% were CD31-positive (endothelial cells, leukocytes, etc.) and 30% were identified as macrophages. Almost all (95%) of the event population identified as macrophages was Cy5-positive (Fig. 8B). Thus, a trend similar to that of the in vitro ferritin internalization by murine macrophages was observed. Atherosclerotic mouse models are characterized by an increased macrophage content at the lesion site. Uptake of ferritin NPs by lesion macrophages was observed to occur within 1 h of injection. Similar accumulation profiles were not exhibited in control studies with injection of dye alone. However, studies on the time-dependent ferritin NP localization and their degradation behavior in blood plasma need to be conducted to discern the uptake mechanism and long-term biodistribution of ferritin NPs in vivo.

Discussion

Ferritin NPs were internalized by macrophages in both in vitro and in vivo models. Human and horse spleen ferritins have previously been shown to undergo transferrin-mediated endocytosis in lymphocytes, reticulocytes, and macrophages[25]. Similarly, we have reported competitive inhibition of AfFtnAA uptake in the presence of transferrin, a natural ligand of transferrin receptors[41]. In agreement with these results, our studies show that pretreating cells with chlorpromazine results in an ~22%

reduction in ferritin uptake, suggesting clathrin- or receptor-mediated uptake. However, no single pathway appears to play a dominant role in the internalization of ferritin, as similar extents of uptake inhibition are observed in cells pretreated with caveolae-mediated and macropinocytosis pathway inhibitors. The role of clathrin pits is apparent at a ferritin concentration of 200 nM, suggesting that a certain concentration of NPs is needed for specific receptor interactions and subsequent endocytosis to occur. Such concentration-dependent differences in endocytosis routes have been previously observed for the internalization of membrane receptors and cell-penetrating peptides[42,43]. TfR1-mediated endocytosis is the pathway by which human ferritin is taken up[25]. Similarly, we have reported that *Af* ferritin, given its structural similarities with human ferritin, follows TfR1-mediated endocytosis[41]. Given the structural similarities between the AA modified *Af* ferritin and human ferritin, additional studies are needed to elucidate the functions of other known human ferritin receptors, such as Scara5.

A study by Turris et al. showed that resurfacing AfFtn to mimic the external surface of human ferritin (HumAfFt) results in increased uptake[44]. The authors previously found that the overall amount of ferritin NP internalization (via TfR1) were improved in HeLa cells by introducing residues analogous to those found in heavy chain human ferritin to the 12 amino acid loops exposed on the wild-type *Af* ferritin (AfFtnWT) sequence. We observed a similar 4-fold increase in ferritin internalization using HumAfFt in RAW264.7 cells after 24 h of treatment when compared to ferritin internalization by AfFtnWT and AfFtnAA (Fig. S6). THP-1 human macrophages treated with AfFtnAA also displayed similar uptake in comparison to the murine macrophage models used in this study and were thereby expected to follow similar uptake mechanisms and molecular responses (Fig. S7). To further explore the use of HumAfFt as an alternative to AfFtnAA in drug delivery and MRI applications, the impacts of such modification on the biophysical properties of AfFtnAA (such as iron-binding kinetics) need to be investigated.

The internalization of SPIONs has been shown to be dependent on all three pathways to similar extents[7]. Treatment of macrophages with chlorpromazine, MβCD and amiloride inhibite the uptake of SPIONs. Since ferritin NPs contain iron cores are similar to those of SPIONs in terms of size and structure, our data suggest that the protein shell and bare iron oxide NPs interact with the cell membrane following similar mechanisms, thus resulting in internalization via multiple pathways. An initial increase in Fe accumulation followed by a decrease after 48 h of exposure is observed after treating cells with ferritin NPs. Of particular relevance to our observations, Kim et al. suggest the concept of the dilution of NP concentrations in daughter cells compared to parent cells, as illustrated using polystyrene NPs[45]. This results in a nonlinear trend in internalization wherein the net NP accumulation in the cells eventually plateaus with time. Since the measured Fe accumulation in this study is an average across cells of different generations, a similar deviation from the linear NP uptake trend is expected and observed. The reduction in the amount of accumulated Fe per cell as well as total cellular Fe levels further suggests that iron export occurs with prolonged incubation time.

Ferritin NPs localize to the endosomal compartments following clathrin-mediated uptake. In vitro simulation of lysosomal conditions shows that digestion of the ferritin protein shell occurs in the presence of lysosomal enzymes. Iron core solubilization occurs under strong reducing conditions, with the protein shell remaining intact. Subcellular quantification demonstrates a significant content of iron atoms in the cytoplasmic compartments, which likely corresponds to the ferrous ions resulting from the iron core dissolution. Ferritin NP localization is slightly different from the cellular fate of SPIONs previously studied in RAW264.7 cells[7]. Iron oxide nanoparticles undergo lysosomal degradation pathways similar to those of the free iron pool released in the cytoplasm[7]. Interestingly, a small proportion of intact ferritin NPs are visualized as high-contrast particles in the cytoplasm using electron microscopy. To further elucidate the structural properties of these intact cage structures, advanced techniques such as cryo-EM and EDX could be utilized to further supplement the visualization methods used in this study.

There are similarities between the exogenous ferritin localization data in this study and the localization and degradation pathways of endogenous ferritin synthesized in the cytoplasm in response to Fe incubation[46]. Synthesized ferritin enters lysosomes by binding to the cargo receptor NCO4A in response to iron deprivation. The iron inside these ferritin molecules is then released into the lysosomes in the presence of high concentrations of chelating agents such as glutathione and ascorbic acid[47]. Similar to the endogenous ferritin degradation pathway, our results confirm that protein shell degradation is decoupled from the dissolution of the iron core.

Exogenous ferritin is found to have less impact on iron homeostasis in cells by providing protective effects, likely by slowing the iron core dissolution process. In response to iron release from ferritin NPs, mRNA transcriptional analyses show significant upregulation of endogenous ferritin levels after 48 h of incubation. This suggests the transfer of iron from exogenous ferritin NPs to endogenous heavy- and light-chain ferritins. Furthermore, the upregulation of ferroportin mRNA was observed, validating the activation of the iron export mechanism over 48 h. The regulation of ferroportin, the only known iron exporter protein, is indicative of the effects of ferritin on

iron homeostasis in cells. Excess iron that is released by ferritin degradation induces the production of iron-relevant proteins to maintain iron homeostasis[48,49]. Interestingly, the upregulation of L-ferritin mRNA in the ferritin NP-treated samples in this study is found to be 10-fold lower than that treated with SPION for a similar exposure time of 24 h[7] despite the higher molar iron content (present in the ferritin NP core) used in this study. The upregulation of L-ferritin and H-ferritin levels indicates a protective mechanism against potential oxidative damage in cells due to the production of hydrogen peroxide that occurs during iron release. Although such oxidative damage may not result in cytotoxicity, it could have secondary effects on cellular activities and cause genetic disorders[50]. The lower iron-related molecular responses after ferritin NP treatment presents an advantage over SPIONs for biomedical applications. This study emphasizes the importance of modulating the iron content and treatment duration using ferritin NPs to minimize the impacts on iron homeostasis and potential oxidative stress. This conclusion is further supported in this study by analyzing the immune-related genes in response to ferritin treatment.

As macrophages are part of the first line of defense in the immune response, it is important to study their molecular responses to NPs and monitor their regulation of immunologically relevant genes. To monitor these responses, the fold changes in mRNA expression of CCR2, VCAM-1, IL1β and TNFα were studied. CCR2 and VCAM-1 mediate the increased requirements for leukocytes, macrophage polarization, cell migration and cell adhesion in vivo[51,52]. We observed the upregulation (~6500-fold change) of the proinflammatory cytokine IL1β in response to ferritin NP treatment. Additionally, due to the possibility that the Fe^{3+} core undergoes a change in oxidation state and induces oxidative stress, ROS levels were monitored after different exposure times. Of the four genes analyzed, IL1β was significantly upregulated along with a time-dependent increase in ROS levels. A relationship between the core Fe content and the molecular responses was also detected, as suggested by the less pronounced increase in ROS and immune markers upon treatment with the iron-devoid ApoAA. The inflammasome pathway has been identified as the most common signaling pathway that correlates ROS formation to the subsequent upregulation of IL1β and is associated with the upregulation of the NLRP3 gene. However, in this study, the oxidative stress induced by ferritin NP treatment was determined to be the result of an inflammasome-independent pathway, as no significant changes in the regulation of the NLRP3 gene were found (Fig. S2B)[53,54]. This result highlights the need to further understand the ferritin-specific mode of action that causes these cellular responses and oxidative stress. Our study further explored the possibility of increased oxidative stress as a result of prolonged exposure to the iron atoms in the core of the protein shell. Thus, it is important to tune the Fe content in the particle considering the possible oxidative and immunological responses. This tuning is particularly important in cases where ferritin NPs target diseased tissues and an increase in free radical species or cytokines could result in further disease progression due to inflammation.

Ferritin protein nanocages/nanoparticles have garnered significant research interest as drug delivery vehicles for small molecules, siRNAs, and short peptides among many others[15,55]. The target intracellular space for a large proportion of these therapeutic molecules is the cytoplasm[56]. Based on our study, the majority of the cargo in ferritin (in this case, Fe) localizes in the endosomal compartments followed by its release into the cytoplasmic compartment after protease degradation in the endosomes/lysosomes. However, this delivery mechanism to the cytoplasm would not be feasible with cargo that is sensitive to low pH or proteolytic enzymes in the endosomes and lysosomes. Thus, it is desirable for the carrier to be able to escape from the endosome for direct release of the cargo into the cytoplasm. The two key mechanisms that have been proposed to mediate endosomal escape are the proton sponge theory and charge-mediated membrane disruption[57]. Proton sponge theory refers to the disruption of endosomal compartments due to osmotic swelling via the recruitment of protons that protonate nonexposed amino acid residues in response to the low pH in these organelles[58]. Membrane disruption, on the other hand, is thought to occur due to the interaction of the cationic residues on the endosomal membrane surface, resulting in holes in the lipid bilayer and thereby causing disruption[59]. To overcome the barriers of the endosomal/lysosomal compartments, we attempted to use poly-histidine peptides to mediate the escape of ferritin NPs from these regions. Previous studies have demonstrated the use of histidine-based peptides for the delivery of siRNA and toxins using chitosan, gold nanoparticles and ribonucleotide octamers[39,60,61]. To our knowledge, the study conducted here is the first to attempt endosomal escape by protein NPs. We developed two ferritin conjugates with poly-histidine peptides genetically engineered to the N- (HHEN-AA) and C-termini (AA-HHEC) of the polypeptide. The N-terminus of the polypeptide is exposed on the outer surface while the C-terminus faces the inner cavity, thus differentiating the locations of the peptides on ferritin. These conjugates allowed us to determine whether the favored mechanism of endosomal escape was cationic residue-mediated membrane disruption or the proton sponge effect. A 10% decrease in endosomal/lysosomal iron accumulation was observed at 48 h after HHEN-AA treatment vs. a 5% decrease after AA-HHEC

treatment. This finding indicates that surface poly-histidine peptides play a greater role in membrane disruption and thereby mediate endosomal escape. Further, the protonation of the histidine residues is not a sufficient driving force for the rupture of the endosomal compartments. However, the lower percentage of endosomal escape found here compared to that determined in previous studies is likely because proteins are more vulnerable to lysosomal degradation than hybrid NPs[39]. Transcriptional analysis revealed an ~6-fold increase in L-ferritin in cells incubated with the poly-histidine mutants in comparison to unmodified AA. Despite the lower percentage of cytoplasmic iron accumulation, the greater fold increase in mRNA level was likely observed due to the higher iron content loaded per cage in AA-HHEC. We speculate that the iron loaded in AA-HHEC was first released in the endosome and then escaped into the cytosol, resulting in an early increase in mRNA level. We envision that the endosomal release property presented in this work could be further enhanced by adding cationic amino acid residues on NP surface, as stronger cationic properties are expected to further enhance endosomal membrane disruption. A study of the structural (secondary and tertiary structures) differences between the engineered molecules could further enhance the understanding of endosomal escape and subcellular localization.

Observations from the in vivo studies indicate that 95% of the macrophages in the lesion sites internalized the cages within 1 h, thus demonstrating the passive localization of ferritin to plaque macrophages. The localization of heavy chain human ferritin to lesion sites has been previously reported using fluorescence and MR imaging in an atherosclerotic mouse model[16]. This study agrees with the previously conducted work, reporting similar trends for ferritin NPs derived from different species. Furthermore, this study extends the previous observation by discerning the type of cell that internalizes the NPs in a quantifiable manner. The scope of this work can be widened by conducting longitudinal biodistribution studies and identifying the stability of ferritin NPs in blood plasma to accurately determine the circulation time. Further, additional antibody screening can be used to distinguish between resident macrophages, resident foam cells (cholesterol-laden macrophages) with upregulated TfR1 and circulating macrophages within the lesion site to explore the use of ferritin NPs as macrophage-targeting delivery vehicles for atherosclerosis management.

In conclusion, we analyzed the uptake pathways and cellular localization of ferritin NPs in murine macrophages and determined the molecular responses of the cells to the treatment. We determined that although no single pathway is responsible for ferritin uptake by macrophages, the local particle concentration plays a role in determining the dominant uptake pathway. Subcellular localization studies revealed NP distribution in the endosomal and cytoplasmic compartments. Modulation of intracellular localization to enable greater cytoplasmic accumulation of the cages was demonstrated by engineering the cages with poly-histidine tags. Furthermore, we investigated the process of protein shell degradation in vitro and found that the proinflammatory cytokine IL1β was overexpressed in response to the free Fe ions released from the core. Finally, an in vivo ferritin localization study in an atherosclerotic mouse model showed predominant localization in plaque macrophages. The understanding of ferritin NP internalization and its effects on cellular iron homeostasis provides insights for the design and development of diagnostic and therapeutic tools using ferritin NPs in different disease models.

Materials and methods

AfFtnAA protein production

The AfFtnAA protein was overproduced and purified following previously described methods[28]. Briefly, the E. coli BL21 (DE3) C + RIL was transformed with pET-11a plasmid containing AfFtnAA gene. The culture was induced with 1 mM isopropyl β-d-1-thiogalactopyranoside (IPTG) at $OD_{600} = 0.6–0.8$ and grown for 4 h for protein production. The cells were harvested and lysed by sonication (Sonics Ultrasonic Processor VCX500). The lysates were heat-treated at 85 °C for 10 min and ultracentrifuged (Beckman Coulter Optima L-100XP) at 235,000 × *g* for 1 h. Hydrophobic interaction chromatography (HiTrap Phenyl FF (High Sub), GE/Cytiva) using an AKTA Pure system (GE/Cytiva) was carried out on the soluble fraction to obtain pure protein. The average 280/260 absorbance ratio indicating purity was ~1.7. Fe2400 atoms were used to mediate the self-assembly of Apo AfFtnAA (dimeric form) to generate the cage structure (24mer). Excess iron was removed using a PD-10 desalting column (GE/Cytiva).

Cell culture

RAW264.7 murine macrophages (ATCC) were grown in DMEM (Life Technologies) supplemented with 10% fetal bovine serum and 1% penicillin–streptomycin (Gibco).

Confocal imaging

AfFtnAA was labeled with fluorescein isothiocyanate (FITC; Sigma), used in 100 molar excess, and dialyzed against 25 mM HEPES and 50 mM NaCl, pH 7.4, to remove unreacted dye. Approximately 1 molecule of FITC was conjugated per AfFtnAA cage as determined by a fluorescence standard curve. Cells mounted on a slide was incubated with FITC-AfFtnAA for 24 h. Lysosomes were labeled with LysoTracker™ Red DND-99 (Life Technologies), and the nuclei were labeled with

4′,6-diamidino-2-phenylindole (DAPI; Life Technologies). An LSM800 confocal microscope (Carl Zeiss) was used to observe the mounted samples with a 100× objective at excitation $\lambda = 408$ nm, 488 nm and 594 nm corresponding to DAPI, FITC and LysoTracker™, respectively.

Endocytosis pathway

Cells were pretreated with 15 μM chlorpromazine hydrochloride, 385 μM genistein and 165 μM amiloride hydrochloride hydrate prepared in cell culture media as clathrin-mediated, caveolae-mediated, and macropinocytosis pathway inhibitors, respectively for 1 h under typical cell culture conditions. The media was then aspirated, and the cells were washed with PBS and treated with the indicated concentration of AfFtnAA for 2 h. The degree of internalization by AfFtnAA was quantified using ICP–MS. The amount of Fe detected in the cells was normalized to that in cells treated with AfFtnAA (without inhibitor pretreatment) to obtain the % uptake inhibition for each condition.

Subcellular fractionation

Density-based centrifugation was performed to isolate the cellular organelles following protocols described previously[46,62]. Briefly, differential centrifugation at $1000 \times g$ (5 min), $10{,}000 \times g$ (10 min) and $100{,}000 \times g$ (1 h) was performed to isolate debris, lysosomes/endosomes and the cell membrane in the pellet fraction, respectively. The lysis buffer consisted of 250 mM sucrose, 20 mM HEPES, 10 mM KCl, 1.5 mM $MgCl_2$, 1 mM EDTA, 1 mM DTT and 1 mM protease inhibitor cocktail. The supernatant from the final centrifugation was collected as the cytoplasmic fraction. Lysosomes were further isolated from the lysosome/endosome mixture by centrifugation at $15{,}000 \times g$ for 15 min in the presence of Triton X-100 and 1 mM DTT. The pellets and supernatant fractions were digested with 3% v/v HNO_3 in Milli-Q water to determine the iron concentrations using inductively coupled plasma–mass spectrometry (ICP–MS). The amounts of iron in the total cell pellets, prepared according to the above procedure, and culture medium were determined by ICP–MS as described above.

Transmission electron microscopy (TEM)

Cells were fixed and sectioned following protocols previously described with slight adjustments[63]. Briefly, cells were washed 3 times with PBS and collected using trypsin after AfFtnAA treatment (200 nM for 24 h). The cell pellets were fixed overnight with a mixture of 4% paraformaldehyde and 2.5% glutaraldehyde in PBS, post-fixed using 2% osmium tetroxide (OsO_4; Sigma Aldrich) at room temperature for 2 h, and washed with DI to remove the fixative. Dehydration of the pellets was performed with an ascending series of ethanol (25%, 50%, 75%, 95% and 100%) and pure acetone for 40 min each time at room temperature. Infiltration with resin (Araldite 502 kit, Ted Pella) was started at room temperature with a mixture of acetone and resin at ratios of 1:1, 1:3 and 1:6 for 2 h, 1 h and overnight, respectively. Cell pellets were transferred to fresh resin at room temperature (1 h of incubation) and transferred again to more fresh resin for incubation at 40 °C for 1 h. The same process was repeated at 45 °C and 50 °C. The cell pellets were finally embedded into resin in a polyurethane mold and incubated at 60 °C for at least 48 h. The cell pellet-embedded capsules were sectioned at a thickness of 70 to 100 nm with an ultramicrotome using a diamond knife and collected on copper grids (EMS). The sections on the copper grids were stained with 2% uranyl acetate and lead citrate for 8 min each at room temperature and viewed using a Carl Zeiss Libra microscope with an accelerating voltage of 120 kV.

In vitro simulation of AfFtnAA lysosomal degradation

Lysosomal degradation of AfFtnAA was simulated and measured using an iron release kinetics assay at 37 °C. Degradation was simulated under low pH conditions (4.5), reducing conditions (in the presence of 5 mM DTT, 5 mM EDTA) and in the presence of lysosomal enzyme (1 unit of cathepsin-B). The rate at which iron was release with the degradation of the core was studied by the reaction between ferrozine and the reduced Fe^{2+} formed after core degradation, resulting in the formation of a complex with an absorbance peak at $\lambda = 562$ nm. Then, 200 nM (Fe2400) AfFtnAA was incubated with different buffers in the presence of 1 mM ferrozine (Sigma). Iron release was monitored for 1 h in the presence of reducing agents or 14 h in the presence of protease under different pH conditions. Degraded iron cores and protein shell structures were further examined using TEM with and without uranyl acetate staining.

Real-time PCR

To analyze the effect of ferritin on the mRNA expression of various proteins involved in iron metabolism, real-time qPCR was performed. Cells were incubated with 200 nM AfFtnAA for 12 h, 24 h and 48 h. Untreated cells were used as the negative control. Total RNA was isolated from the cell pellets using an EZ-10 DNAaway RNA Miniprep kit (Biobasic) following the manufacturer's instructions. The RNA concentration was measured using a NanoDrop spectrophotometer (ND-1000) at $\lambda = 260$ nm. One hundred nanograms of RNA from each sample was used along with a Luna® Universal One-Step RT–qPCR kit (NEB) to perform RT–qPCR. The primers used are summarized in Table S1. The reactions were performed in a 20 μL reaction volume using the

STepOne plus Real-time PCR system (Applied Biosystems). The cycle threshold (CT) values for the target genes were determined and normalized relative to β-actin. The fold change in mRNA expression was calculated following the $2^{-\Delta\Delta CT}$ method.

Expression and cloning of poly-histidine-modified AfFtnAA

The AfFtnAA gene was genetically modified by fusing $(HHE)_9$ at the C- and N-termini to construct the two plasmids. GGGS was inserted as a flexible linker between the native protein and the histidine-containing peptide. The plasmids were inserted into the E. coli BL21 C + RIL strain. Proteins were produced following the same protocols as the native protein with slight variations. After cell lysis, protein-containing supernatants were heat-treated at 75 °C for 10 min before ultracentrifugation. HisTrap chromatography (HP) was performed using an AKTA Pure fast protein liquid chromatography system (GE/Cytvia) to purify the proteins. Proteins were eluted with 25 mM HEPES, 50 mM NaCl, and 500 mM imidazole at pH 7.5, and the buffer was exchanged to remove excess imidazole. Self-assembly for cage formation was mediated using Fe1200 atoms.

Reactive oxygen species measurements

After treatment with ferritin under different conditions, the cells were washed thrice with PBS followed by incubation with dihydroethidium hydrochloride (DHE) (Life Technologies) diluted in cell culture media to a working concentration of 5 μM for 1 h at 37 °C. A 10 mM DHE stock solution was prepared in DMSO. Excess dye was washed away with PBS (3 times). The mean fluorescence intensities of the scraped cell samples were measured using a flow cytometer (BD Fortessa X20) at Ex 518/Em 606 nm.

Animal details

Approval for the animal model was obtained from the Institute Animal Care and Use Committee (IACUC) at Nanyang Technological University (NTU), and all procedures were performed in accordance with the protocols and guidelines for the 'Use of Animals'. $ApoE^{-/-}$ mice used for IVIS and flow cytometry were fed a high-fat diet from 10 weeks after birth to 17 weeks before use in the experiment.

In vivo biodistribution (IVIS) of the aorta

$ApoE^{-/-}$ mice were administered a single bolus dose (1 mg/kg) of Cy5-labeled ferritin through a lateral tail vein. One hour post-injection, the mice were euthanized and perfused with 20 mL of PBS/mouse via cardiac puncture, and the aorta was excised. The organs and aorta were imaged using an ex vivo near-infrared fluorescence (NIRF) imaging system.

Flow cytometry of the digested aortas

Digested aortas were analyzed following previously described protocols[64]. Aortas extracted from five mice were digested with 1 mg/ml collagenase IV in Hank's balanced salt solution (HBSS) at 37 °C for 60 min at room temperature and filtered through a 160 μm nylon mesh to obtain a cell suspension. The cells were washed with fluorescence-activated cell sorting (FACS) buffer solution before being suspended and incubated with a mixture of macrophage-specific antibody cocktails for 30 min at 4 °C. The antibody cocktails (BioLegend) included CD45 (clone 30-F11), CD11b (clone M1/70), CD64 (clone X54-5/7.1), F4/80 (clone BM8), MerTK (R&D Systems) and CD31 (clone ER-MP12) (Bio-Rad), which were tagged with nonoverlapping fluorescent particles at different wavelengths. Fluorescence was detected using a flow cytometer (BD Biosciences LSRFortessa X-20), and the data were analyzed using BDFacsDiva and FlowJo software. Macrophages from aortas were identified as trypan blue- CD45 + CD11b + MerTK+ CD64 + F4/80 +. The population identified as CD31 + was used to identify the group of cells emitting Cy5 fluorescence and excluded the Cy5 fluorescence in the population identified as macrophages.

Acknowledgements

This work is supported in parts by Nanyang Technological University, Singapore Start-Up Grant through the School of Materials Science and Engineering and Institute for Digital Molecular Analytics and Science (IDMxS) at Nanyang Technological University, Singapore through Singapore Ministry of Education funding under the Research Centres of Excellence scheme. We thank Prof. Beatrice Vallone of the Institute of Molecular Biology and Pathology, National Research Council, Italy for gifting HumAfFt.

Author details

[1]School of Chemistry, Chemical Engineering and Biotechnology, Nanyang Technological University, Jurong West, Singapore. [2]School of Materials Science and Engineering, Nanyang Technological University, Jurong West, Singapore. [3]Environmental Chemistry and Materials Centre, Nanyang Environment and Water Research Institution, Nanyang Technological University, Jurong West, Singapore. [4]Lee Kong Chian School of Medicine (LKC), Nanyang Technological University, Jurong West, Singapore. [5]Institute for Digital Molecular Analytics and Science (IDMxS), Nanyang Technological University, Jurong West, Singapore

Author contributions

SR: protein design and production (various ferritin constructs in the work), in vitro experiments involving cellular treatment, data analysis, and manuscript writing. SL: conceptualization, funding acquisition, data analysis, and manuscript editing. AMN, BC: Animal experiments and analysis (in vivo biodistribution and flow cytometry). AG, KWN: Cell transmission electron microscopy and analysis.

Conflict of interest

The authors declare no competing interests.

Supplementary information The online version contains supplementary material available at https://doi.org/10.1038/s41427-022-00453-w.

Received: 7 August 2021 Revised: 17 July 2022 Accepted: 3 August 2022.
Published online: 13 January 2023

References

1. Behzadi, S. et al. Cellular uptake of nanoparticles: journey inside the cell. *Chem. Soc. Rev.* **46**, 4218–4244 (2017).
2. Gustafson, H. H., Holt-Casper, D., Grainger, D. W. & Ghandehari, H. Nanoparticle uptake: the phagocyte Problem. *Nano Today* **10**, 487–510 (2015).
3. Kettler, K., Giannakou, C., de Jong, W. H., Hendriks, A. J. & Krystek, P. Uptake of silver nanoparticles by monocytic THP-1 cells depends on particle size and presence of serum proteins. *J. Nanopart. Res* **18**, 286 (2016).
4. Liu, Y., Hardie, J., Zhang, X. & Rotello, V. M. Effects of engineered nanoparticles on the innate immune system. *Semin Immunol.* **34**, 25–32 (2017).
5. Sharma, G., She, Z. G., Valenta, D. T., Stallcup, W. B. & Smith, J. W. Targeting of macrophage foam cells in atherosclerotic plaque using oligonucleotide-functionalized nanoparticles. *Nano Life* **1**, 207–214 (2010).
6. Cieslewicz, M. et al. Targeted delivery of proapoptotic peptides to tumor-associated macrophages improves survival. *Proc. Natl Acad. Sci. USA* **110**, 15919–15924 (2013).
7. Gu, J. et al. The internalization pathway, metabolic fate and biological effect of superparamagnetic iron oxide nanoparticles in the macrophage-like RAW264.7 cell. *Sci. China Life Sci.* **54**, 793–805 (2011).
8. Chithrani, B. D., Ghazani, A. A. & Chan, W. C. Determining the size and shape dependence of gold nanoparticle uptake into mammalian cells. *Nano Lett.* **6**, 662–668 (2006).
9. Chithrani, B. D. & Chan, W. C. Elucidating the mechanism of cellular uptake and removal of protein-coated gold nanoparticles of different sizes and shapes. *Nano Lett.* **7**, 1542–1550 (2007).
10. Champion, J. A. & Mitragotri, S. Role of target geometry in phagocytosis. *Proc. Natl Acad. Sci. USA* **103**, 4930–4934 (2006).
11. Skajaa, T. et al. High-density lipoprotein-based contrast agents for multimodal imaging of atherosclerosis. *Arterioscler Thromb. Vasc. Biol.* **30**, 169–176 (2010).
12. Greish, K. Enhanced permeability and retention (EPR) effect for anticancer nanomedicine drug targeting. *Methods Mol. Biol.* **624**, 25–37 (2010).
13. Su, Y.L. & Hu, S.H. Functional nanoparticles for tumor penetration of therapeutics. *Pharmaceutics*. **10**, 193 (2018).
14. Lee, L. A. & Wang, Q. Adaptations of nanoscale viruses and other protein cages for medical applications. *Nanomedicine* **2**, 137–149 (2006).
15. Bhaskar, S. & Lim, S. Engineering protein nanocages as carriers for biomedical applications. *NPG Asia Mater.* https://doi.org/10.1038/am.2016.128 (2017).
16. Truffi, M. et al. Ferritin nanocages: A biological platform for drug delivery, imaging and theranostics in cancer. *Pharm. Res* **107**, 57–65 (2016).
17. Terashima, M. et al. Human ferritin cages for imaging vascular macrophages. *Biomaterials* **32**, 1430–1437 (2011).
18. Sana, B., Johnson, E., Sheah, K. Poh, C. L. & Sierin, L. Iron-based ferritin nanocore as a contrast agent. *Biointerphases* **5**, 48–52 (2010).
19. Sana, B., Poh, C. L. & Lim, S. A manganese-ferritin nanocomposite as an ultrasensitive T2 contrast agent. *Chem. Commun. (Camb.)* **48**, 862–864 (2012).
20. Zhao, Y. et al. Bioengineered magnetoferritin nanoprobes for single-dose nuclear-magnetic resonance tumor imaging. *ACS Nano* **10**, 4184–4191 (2016).
21. Khoshnejad, M. et al. Ferritin nanocages with biologically orthogonal conjugation for vascular targeting and imaging. *Bioconjugate Chem.* **29**, 1209–1218 (2018).
22. Khoshnejad, M. et al. Vascular accessibility of endothelial targeted ferritin nanoparticles. *Bioconjugate Chem.* **27**, 628–637 (2016).
23. Palombarini, F., Di Fabio, E., Boffi, A., Macone, A. & Bonamore, A. Ferritin nanocages for protein delivery to tumor cells. *Molecules*. **25**, 825 (2020).
24. Khoshnejad, M., Parhiz, H., Shuvaev, V. V., Dmochowski, I. J. & Muzykantov, V. R. Ferritin-based drug delivery systems: hybrid nanocarriers for vascular immunotargeting. *J. Control Release* **282**, 13–24 (2018).
25. Li, L. et al. Binding and uptake of H-ferritin are mediated by human transferrin receptor-1. *Proc. Natl Acad. Sci. USA* **107**, 3505–3510 (2010).
26. Ramm, G. A., Ruddell, R. G. & Subramaniam, V. N. Identification of ferritin receptors: their role in iron homeostasis, hepatic injury, and inflammation. *Gastroenterology* **137**, 1849–1851 (2009).
27. Sana, B., Johnson, E. & Lim, S. The unique self-assembly/disassembly property ofArchaeoglobus fulgidus ferritin and its implications on molecular release from the protein cage. *Biochim Biophys. Acta* **1850**, 2544–2551 (2015).
28. Sana, B. et al. The role of nonconserved residues of *Archaeoglobus fulgidus* ferritin on its unique structure and biophysical properties. *J. Biol. Chem.* **288**, 32663–32672 (2013).
29. Chakraborti, S. et al. Three-dimensional protein cage array capable of active enzyme capture and artificial chaperone activity. *Nano Lett.* **19**, 3918–3924 (2019).
30. Tetter, S. & Hilvert, D. Enzyme encapsulation by a ferritin cage. *Angew. Chem. Int. Ed.* **56**, 14933–14936 (2017).
31. Pulsipher, K. W., Bulos, J. A., Villegas, J. A., Saven, J. G. & Dmochowski, I. J. A protein-protein host-guest complex: thermostable ferritin encapsulating positively supercharged green fluorescent protein. *Protein Sci.* **27**, 1755–1766 (2018).
32. Guo, J. et al. Efficient expression of recombinant human heavy chain ferritin (FTH1) with modified peptides. *Protein Expr. Purif.* **131**, 101–108 (2017).
33. Kim, M. et al. pH-dependent structures of ferritin and apoferritin in solution: disassembly and reassembly. *Biomacromolecules* **12**, 1629–1640 (2011).
34. Kumari, S., Mg, S. & Mayor, S. Endocytosis unplugged: multiple ways to enter the cell. *Cell Res.* **20**, 256–275 (2010).
35. Hu, Y. B., Dammer, E. B., Ren, R. J. & Wang, G. The endosomal-lysosomal system: from acidification and cargo sorting to neurodegeneration. *Transl. Neurodegener.* **4**, 18 (2015).
36. McGlinchey, R. P. & Lee, J. C. Cysteine cathepsins are essential in lysosomal degradation of alpha-synuclein. *Proc. Natl Acad. Sci. USA* **112**, 9322–9327 (2015).
37. Stoka, V., Turk, B. & Turk, V. Lysosomal cysteine proteases: structural features and their role in apoptosis. *IUBMB Life* **57**, 347–353 (2005).
38. Brzicova, T. et al. Molecular responses in THP-1 macrophage-like cells exposed to diverse nanoparticles. *Nanomaterials (Basel).* **9**, 687 (2019).
39. Tai, W., Li, J., Corey, E. & Gao, X. A ribonucleoprotein octamer for targeted siRNA delivery. *Nat. Biomed. Eng.* **2**, 326–337 (2018).
40. Peng, T., Paramelle, D., Sana, B., Lee, C. F. & Lim, S. Designing non-native iron-binding site on a protein cage for biological synthesis of nanoparticles. *Small* **10**, 3131–3138 (2014).
41. Ravishankar, S. & Lim, S. Cyclodextrin conjugated ferritin nanocages reduce intracellular cholesterol level in foam cells. *Nano Res.* **12**, 2925–2932 (2019).
42. Aguilar, R. C. & Wendland, B. Endocytosis of membrane receptors: two pathways are better than one. *Proc. Natl Acad. Sci. USA* **102**, 2679–2680 (2005).
43. Mager, I., Langel, K., Lehto, T., Eiriksdottir, E. & Langel, U. The role of endocytosis on the uptake kinetics of luciferin-conjugated cell-penetrating peptides. *Biochim Biophys. Acta* **1818**, 502–511 (2012).
44. de Turris, V. et al. Humanized archaeal ferritin as a tool for cell targeted delivery. *Nanoscale* **9**, 647–655 (2017).
45. Kim, J. A., Aberg, C., Salvati, A. & Dawson, K. A. Role of cell cycle on the cellular uptake and dilution of nanoparticles in a cell population. *Nat. Nanotechnol.* **7**, 62–68 (2011).
46. Truman-Rosentsvit, M. et al. Ferritin is secreted via 2 distinct nonclassical vesicular pathways. *Blood* **131**, 342–352 (2018).
47. La, A. et al. Mobilization of iron from ferritin: new steps and details. *Metallomics* **10**, 154–168 (2018).
48. Sabelli, M. et al. Human macrophage ferroportin biology and the basis for the ferroportin disease. *Hepatology* **65**, 1512–1525 (2017).
49. Ward, D. M. & Kaplan, J. Ferroportin-mediated iron transport: expression and regulation. *Biochim Biophys. Acta* **1823**, 1426–1433 (2012).
50. Arosio, P. & Levi, S. Ferritin, iron homeostasis, and oxidative damage1,2 1Guest Editor: Mario Comporti 2This article is part of a series of reviews on "Iron and Cellular Redox Status." The full list of papers may be found on the homepage of the journal. *Free Radic. Biol. Med.* **33**, 457–463 (2002).
51. Bakos, E. et al. CCR2 regulates the immune response by modulating the interconversion and function of effector and regulatory T cells. *J. Immunol.* **198**, 4659–4671 (2017).
52. Grome, H. N. et al. Association of T cell and macrophage activation with arterial vascular health in HIV. *AIDS Res Hum. Retroviruses* **33**, 181–186 (2017).
53. Dai, J., Zhang, X., Li, L., Chen, H. & Chai, Y. Autophagy inhibition contributes to ROS-producing NLRP3-dependent inflammasome activation and cytokine secretion in high glucose-induced macrophages. *Cell Physiol. Biochem* **43**, 247–256 (2017).

54. Yang, Y., Wang, H., Kouadir, M., Song, H. & Shi, F. Recent advances in the mechanisms of NLRP3 inflammasome activation and its inhibitors. *Cell Death Dis.* **10**, 128 (2019).
55. Lee, E. J. et al. Engineered proteinticles for targeted delivery of siRNA to cancer cells. *Adv. Funct. Mater.* **25**, 1279–1286 (2015).
56. Parodi, A. et al. Enabling cytoplasmic delivery and organelle targeting by surface modification of nanocarriers. *Nanomed. (Lond.)* **10**, 1923–1940 (2015).
57. Bus, T., Traeger, A. & Schubert, U. S. The great escape: how cationic polyplexes overcome the endosomal barrier. *J. Mater. Chem. B* **6**, 6904–6918 (2018).
58. Boussif, O. et al. A versatile vector for gene and oligonucleotide transfer into cells in culture and in vivo: polyethylenimine. *Proc. Natl Acad. Sci. USA* **92**, 7297–7301 (1995).
59. Vaidyanathan, S., Orr, B. G. & Banaszak Holl, M. M. Role of cell membrane-vector interactions in successful gene delivery. *Acc. Chem. Res* **49**, 1486–1493 (2016).
60. Sun, P. et al. siRNA-loaded poly(histidine-arginine)6-modified chitosan nanoparticle with enhanced cell-penetrating and endosomal escape capacities for suppressing breast tumor metastasis. *Int J. Nanomed.* **12**, 3221–3234 (2017).
61. Plaza-Ga, I. et al. pH-triggered endosomal escape of pore-forming Listeriolysin O toxin-coated gold nanoparticles. *J. Nanobiotechnology* **17**, 108 (2019).
62. Brix, K., Lemansky, P. & Herzog, V. Evidence for extracellularly acting cathepsins mediating thyroid hormone liberation in thyroid epithelial cells. *Endocrinology* **137**, 1963–1974 (1996).
63. Rakshit, M. et al. Hydroxyapatite particles induced modulation of collagen expression and secretion in primary human dermal fibroblasts. *Int J. Nanomed.* **15**, 4943–4956 (2020).
64. Darwitan, A. et al. Liposomal nanotherapy for treatment of atherosclerosis. *Adv. Health. Mater.* **9**, e2000465 (2020).